Two-dimensional scale-dependent Rayleigh-Taylor dynamics with variable acceleration in a finite-size domain

By H. Hwang AND S. I. Abarzhi†

1. Motivation and objectives

Rayleigh-Taylor instability (RTI) occurs at the interface of two fluids with different densities when acceleration is in opposite direction to the gradient of the density. RTI has been of significant interest since it spans a variety of types of flows in a wide range of physical scales, such as inertial confinement fusion (Regan *et al.* 2012), supernova (Abarzhi *et al.* 2018), and even galactic scales (Novak *et al.* 2011). The consequence of RTI leading to interpenetration and mixing of the two fluids is a critical element to the evolution of the flows. Therefore, previous studies focused on the prediction of early- and late-time dynamics of the large coherent structure of RTI.

RTI with a single-scale perturbation, whose dominant length scale is determined by the initial condition, is often studied for its evolution process. Significant success was achieved recently in understanding the theory of RTI and Rayleigh-Taylor (RT) mixing with constant acceleration (Abarzhi *et al.* 2013; Abarzhi 2019). Moreover, RTI is extensively investigated in both experiments (Jacobs & Catton 1988; Olsona & Jacobs 2009) and simulations (Cook & Dimotakis 2001; Ramaprabhu *et al.* 2012). In the linear regime of RTI, perturbation grows exponentially in time. Then, the flow transits to the nonlinear regime where the growth of perturbation follows a power-law in time, thus resulting in a relative slower evolution of the instability compared to the linear regime (Abarzhi 2008, 2010). At this stage, the interface transforms into large-scale structures. These structures are bubbles and spikes, which correspond to the portion of lighter fluid penetrating the heavier fluid and vice versa. Along with the growth of bubbles and spikes, small-scale vortical structures emerge due to the shear across the interface. The resulting enhanced interaction and coupling of scales lead to fluid mixing, which is believed to be self-similar to the dimensional analysis (Anuchina *et al.* 2012; Youngs 1984).

As diagnostic parameters characterizing each stage of RTI evolution, the growth rate and the curvature at the bubble and spike fronts are of critical interest. Thus, the development of the models predicting the aforementioned quantities serves the main objective of prior studies. Alon *et al.* (1995) propose the power-laws and similarity solutions for RT and Richtmyer-Meshkov (RM) mixing fronts for all ranges of density ratio. Goncharov (2002) suggests the analytical model for bubble evolution in the nonlinear regime over various Atwood number as an extension of the Layzer thoery (Layzer 1955), which assumed a single-fluid system. However, the limitations and failure cases of the models are reported by Mikaelian (2008).

Also, RT-related phenomena often ensue with variable acceleration rather than a constant acceleration in realistic circumstances (Meshkov 2013; Swisher *et al.* 2015). In supernova blast the acceleration is induced by strong variable shocks, and RT mixing with

† University of Western Australia, Australia.

variable acceleration enables the conditions for the synthesis of heavy and intermediate mass elements (Abarzhi *et al.* 2018). In nano-fabrication, the transformation of materials under a high strain rate is governed by RTI with variable acceleration. Prompted by many realistic applications, RTI with time-varying acceleration is navigated both by experiments (Dimonte & Schneider 1996) and by theory (Hill *et al.* 2019). A recent study by Abarzhi & Williams (2020) describes the dynamics of 3D-hexagonal RTI with acceleration of the power-law in time in the infinite domain.

In the present study, we illustrate the analytic expression of RTI bubbles with time-varying acceleration in a finite-size domain. The group theory is implemented to describe the solutions in a unit cell of 2D spatially periodic flow. Diagnostic parameters not only the curvature and the growth rate but also the interfacial shear are evaluated at the bubble front. The effect of the Atwood number and the domain size is demonstrated. Moreover, we seek the interplay of both horizontal and vertical length scales in nonlinear regime solutions. The universal scale is proposed to bridge the solutions of the finite-size domain to those of infinite-size domain.

2. Methodology

In this section, the governing equations and the boundary conditions are introduced. Then, the fluid potentials satisfying the governing equations and boundary conditions are sought by employing the group theory. A dynamical system is derived to compute diagnostic parameters at the bubble front.

2.1. *Boundary value problem*

The equations governing RTI of incompressible and inviscid fluids are conservation laws of mass, momentum and energy,

$$\frac{\partial \rho}{\partial t} + \frac{\partial \rho v_i}{\partial x_i} = 0, \tag{2.1a}$$

$$\frac{\partial \rho v_i}{\partial t} + \frac{\partial \rho v_i v_j}{\partial x_j} + \frac{\partial P}{\partial x_i} = 0, \tag{2.1b}$$

$$\frac{\partial E}{\partial t} + \frac{\partial (E+P) v_i}{\partial x_i} = 0, \tag{2.1c}$$

in a spatial coordinate system where $(x_1, x_2, x_3) = (x, y, z)$ such that x and y constitute the horizontal plane which is vertical to the acceleration and z represents vertical space. t denotes time, and density, velocity, pressure and energy are introduced as $(\rho, \mathbf{v}, P, E)$, respectively, with v being $\mathbf{v} = (v_1, v_2, v_3)$. The energy E is of the form $E = \frac{1}{2}\rho(e + \mathbf{v}^2/2)$, where e is the internal energy. Note that the conservation equations above describe each of the two different fluids. The effect of surface tension is beyond the scope of the present study and thus not considered here.

In a laboratory frame, the boundary conditions at the end of the domain are

$$v_3(y = Z) = 0, \qquad v_3(y = -Z) = 0, \tag{2.2}$$

where Z is a vertical extent of the two boundaries. The governing equations in Eq. (2.1) together with the boundary conditions in Eq. (2.2) pose a well-defined RTI problem.

The governing equations are transformed into boundary conditions at the interface by introducing a continuous local scalar function, $\theta(x, y, z, t)$. The scalar function $\theta(x, y, z, t)$

is assumed to have a gradient $\nabla\theta$ and the time derivative $\dot{\theta}$ and is given in the form

$$\theta(x,y,z,t) = \begin{cases} \theta_h(x,y,z,t) > 0, & z > z^*(x,y,t) \\ \theta(x,y,z,t) = 0, & z = z^*(x,y,t) \\ \theta_l(x,y,z,t) < 0, & z < z^*(x,y,t). \end{cases} \tag{2.3}$$

Here, the subscript h and l denote the heavy and light fluids, respectively. Also, $z^*(x,t)$ represents the location of the free interface. Then, the variables $(\rho, \mathbf{v}, P, E)$ over the entire flow field are expressed employing the Heavyside step function $H(\theta)$ as

$$(\rho, \mathbf{v}, P, E) = H(\theta)(\rho, \mathbf{v}, P, E)_h + H(-\theta)(\rho, \mathbf{v}, P, E)_l. \tag{2.4}$$

Moreover, it is possible to define interface normal vector $\mathbf{n}$ and interface tangential vector τ using the scalar function $\theta(x,y,z,t)$ as $\mathbf{n} = \nabla\theta/|\nabla\theta|$ and $\mathbf{n}\cdot\tau = 0$. In order to reformulate the governing equations in Eq. (2.1) to interface boundary conditions, we further introduce a mass flux vector $\widetilde{\mathbf{j}}$ across the moving interface $z^*(x,y,t)$ as $\widetilde{\mathbf{j}} = \rho\left(\mathbf{n}\dot{\theta}/|\nabla\theta| + \mathbf{v}\right)$. Substituting Eq. (2.4) for Eq. (2.1) and manipulating the terms using the interface normal and tangential vectors, $\mathbf{n}$ and τ, and a mass flux $\widetilde{\mathbf{j}}$ yield the following interface boundary conditions

$$\left[\widetilde{\mathbf{j}}\cdot\mathbf{n}\right] = 0, \quad \left[\left(P + \frac{(\widetilde{\mathbf{j}}\cdot\mathbf{n})^2}{\rho}\right)\mathbf{n}\right] = 0, \quad \left[(\widetilde{\mathbf{j}}\cdot\mathbf{n})\frac{(\widetilde{\mathbf{j}}\cdot\tau)}{\rho}\tau\right] = 0, \quad \left[(\widetilde{\mathbf{j}}\cdot\mathbf{n})\left(W + \frac{\widetilde{\mathbf{j}}^2}{2\rho^2}\right)\right] = 0. \tag{2.5}$$

The angle brackets on a variable χ denote the difference of χ across the interface, $[\chi] = \chi_h - \chi_l$. Note that the conditions in Eq. (2.5) are derived from the conservation of mass, vertical momentum, horizontal momentum and energy, respectively.

The immiscibility of the fluids at the interface further simplifies Eq. (2.5). The mass flux $\widetilde{\mathbf{j}}$ across the interface in Eq. (2.5) for immiscible fluids poses $\widetilde{\mathbf{j}}\cdot\mathbf{n}|_{\theta=0^\pm} = 0$. We note that this condition corresponds to contact discontinuity. Due to this contact discontinuity, the conditions in Eq. (2.5) are written as

$$[\mathbf{v}\cdot\mathbf{n}] = 0, \quad [P] = 0, \quad [\mathbf{v}\cdot\tau] = arbitrary, \quad [W] = arbitrary. \tag{2.6}$$

The first two conditions in Eq. (2.6) represent the continuity of the normal velocity and the normal pressure, whereas the last two illustrate discontinuity of the tangential velocity and the enthalpy across the interface, respectively.

2.2. *Time varying acceleration*

In the present study, the acceleration, $\mathbf{g}(t)$, is directed from the heavy fluid to the light fluid and varies with time as a power-law function,

$$\mathbf{g}(t) = -Gt^a\hat{z}, \quad t > 0, \tag{2.7}$$

where G is the pre-factor of the dimension $[m/s^{a+2}]$ and a is the dimensionless acceleration exponent that ranges $a \in [-\infty, \infty]$. It is worth emphasizing that for time-varying acceleration as a power-law function, the time scale and the early-time dynamics are distinguished by the acceleration exponent a. If $a > -2$, the acceleration $\mathbf{g}(t)$ determines the time scale and early-time dynamics, and this type of instability is termed RT-type instability. If $a < -2$, the initial condition, such as initial growth rate, controls the time scale and early-time dynamics, and this type of instability is termed RM-type instability. Here, we focus only on RT-type instability ($a > -2$).

2.3. *Group theory*

The group theory approach exploits space groups. Due to the spatial periodicity of RTI, RT dynamics are invariant with respect to the Fedorov and/or Schoenflies group, **G**. The generators of this Fedorov group **G** are translations in the horizontal plane, rotations and reflections. The space groups are classified with respect to the dimensionality: there are 7 one-dimensional and 17 two-dimensional crystallographic groups (Landau & Lifshitz 1987). However, not all space groups are considered here because the structure stability and isotropy significantly limit the types of space groups. Therefore, the space groups that satisfy the following requirements are selected. Firstly, the space groups must have the anisotropy in the acceleration direction and the inversion in the plane normal to the periodic plane. Secondly, the space groups are structurally stable, and thus, the coherent structures are observable and repeatable. The two requirements physically imply that the large-scale fluctuation does not alter the space group **G** and the corresponding dominant wave vector. Consideration of the structure stability and isotropy leaves pm11 for 2D RTI among the crystallographic groups following international classification and Fedorov's notation for space groups.

2.4. *Fourier series expansions*

Due to the aforementioned requirements, the irreducible representation of symmetry group pm11 allows the application of the Fourier series in combination with the generators of **G** to solve the governing equations. For instance, the translational symmetric in x direction by $x+\lambda \to x$, where λ is a spatial period, or equivalently the wavelength of the initial perturbation, introduces the $\sin(kx)$ and $\cos(kx)$ for the odd and even functions, respectively. Note that k is a wavenumber $k = 2\pi/\lambda$ of an initial perturbation that can be arbitrarily chosen.

The large-scale flow are irrotational in the fluid bulk. Therefore, the Fourier series of the fluid potential $\Phi_{h,l}$ with the space group pm11 are expressed as

$$\Phi_h(x,z,t) = \sum_{m=1}^{\infty} \Phi_m(t) \left(z\sinh(mkZ) + \frac{\cos(mkx)}{mk}\cosh[mk(z-Z)] \right) + f_h(t) + c.c, \tag{2.8a}$$

$$\Phi_l(x,z,t) = \sum_{m=1}^{\infty} \widetilde{\Phi}_m(t) \left(-z\sinh(mkZ) + \frac{\cos(mkx)}{mk}\cosh[mk(z+Z)] \right) + f_l(t) + c.c, \tag{2.8b}$$

where $\Phi_m(t)$ and $\widetilde{\Phi}_m(t)$ are, respectively, the Fourier amplitudes of heavy and light fluids of the order m. $f_h(t)$ and $f_l(t)$ are time-dependent functions and $c.c$ are cross-terms. We note that the velocity is related to the fluid potentials as $\mathbf{v}_{h,l} = \nabla\Phi_{h,l}$ and the continuity condition is automatically satisfied as $\Delta\Phi_{h,l} = 0$. Also, y coordinate is eliminated for pm11 due to the dimensional considertation.

The symmetry of the flow affects the form of the interface morphology of bubbles. As mentioned earlier, the dynamics of the large coherent structure at the tips of bubbles are of interest in this study. To this aim, the *pm1* generator $x \to -x$ must be considered for the pm11 space group at the vicinity of the bubbles front. Therefore, the spatial expansions of interface $z^*(x,t)$ with the symmetry constraints only permit

$$z^*(x,t) = \sum_{i=0}^{\infty} \zeta_i x^{2i}. \tag{2.9}$$

2.5. *Dynamical system: 2D pm11*

For a given symmetry group pm11, the irreducible representation and project operators with infinite Fourier series enable the velocity potentials Φ_h and Φ_l to be expanded as forms of Eq. (2.8). In addition, the interface in Eq. (2.9) can be expanded at a vicinity of the tips of bubbles in a given unit cell. Further substitution of the fluid potentials in Eq. (2.8) and the interface in Eq. (2.9) for the governing equations in Eq. (2.6) leads to a dynamical system in terms of moments, M, N, and surface variables ζ_1.

For pm11, the moments M, N are defined as an infinite sum of weighted Fourier moments and are written as

$$\left\{M_n, \widetilde{M}_n, N_n, \widetilde{N}_n\right\} = \sum_{m=1}^{\infty} \left\{\Phi_m(t), \widetilde{\Phi}_m(t), \Phi_m(t), \widetilde{\Phi}_m(t)\right\} (mk)^n \sinh(mkZ), \tag{2.10}$$

where n is integers $n = 1, 2, 3 \ldots$. Note that the moments with a tilde, $\widetilde{M}$ and $\widetilde{N}$, represent moments for light fluid; otherwise, the moments are for heavy fluid. We note that hyperbolic functions appear as a result of finite-size domains.

The pressure term in the first two nontrivial conditions in Eq. (2.6) is replaced by the pressure term in the Bernoulli equation in the accelerating frame with $d\mathbf{v}/dt$, which is

$$\frac{\partial \Phi_{h,l}}{\partial t} = P - \left(\mathbf{g} + \frac{\partial \mathbf{v}}{\partial t}\right) z + \frac{1}{2}(u^2 + v^2) + C(t), \tag{2.11}$$

where $C(t)$ is a function of a time. In addition, the boundary conditions in the accelerating frame are modified as

$$v_2(y = L) = -\mathbf{v}(t) \cdot \hat{\mathbf{e}}_y,\ v_2(y = -L) = -\mathbf{v}(t) \cdot \hat{\mathbf{e}}_y, \tag{2.12}$$

where $\hat{\mathbf{e}}_y$ is a unit vector in y direction. Then, the substitution of moment expressions in Eq. (2.10) and Eq. (2.9) to Eq. (2.6) with Eq. (2.11) and Eq. (2.12) leads to the dynamical system equation. Especially noteworthy is that the dynamical system equations are composed of infinite power series in terms of small x with time-dependent coefficients $\zeta_m(t)$. Thus, the dynamical system can be spatially expanded to the desired order of accuracy.

Finally, the dynamical system for pm11 approximated to $O(x^2)$ is written as

$$\begin{gathered} M_0 + \widetilde{M}_0 = 0, \quad \dot{\zeta}_1 - 3N_1\zeta_1 - \tfrac{M_2}{2} = 0, \quad \dot{\zeta}_1 - 3\widetilde{N}_1\zeta_1 + \tfrac{\widetilde{M}_2}{2} = 0, \\ (1+A)\left(\tfrac{\dot{N}_1}{2} + \zeta_1\dot{M}_0 - \tfrac{N_1^2}{2} - g(t)\zeta_1\right) = (1-A)\left(\tfrac{\dot{\widetilde{N}}_1}{2} - \zeta_1\dot{\widetilde{M}}_0 - \tfrac{\widetilde{N}_1^2}{2} - g(t)\zeta_1\right). \end{gathered} \tag{2.13}$$

$A = (\rho_h - \rho_l)/(\rho_h + \rho_l)$ is the Atwood number and dot notation denotes the time derivative. Note that $M_0 = -\mathbf{v}(t) \cdot \hat{\mathbf{e}}_y$ and $\widetilde{M}_0 = -\mathbf{v}(t) \cdot \hat{\mathbf{e}}_y$.

2.6. *The shear function*

RTI features not only large-scale coherent structures but also secondary instability caused by small-scale vorticies. It is understood that the source of these vorticies is shear developed across the interface. Therefore, shear serves as an important quantity to be parameterized and is of interest in terms of RTI dynamics. The shear function Γ is defined as

$$\Gamma = \lim_{x \to 0} \frac{1}{x} \left(\mathbf{v}_h(x, y) \cdot \tau - \mathbf{v}_l(x, y) \cdot \tau\right) = \widetilde{N}_1 - N_1. \tag{2.14}$$

Note that the working fluids are inviscid in the current study, and thus, no viscous layer exists at a vicinity of the interface. Even though this inviscid framework limits our study to large-scale dynamics, the introduction of shear function allows us to describe qualitative properties of vortical structures and rotation direction, for example, the positive Γ indicating the rotation from the heavy fluid to the light fluid.

3. Results

Our methodology arrives at the dynamical system in Eq. (2.13). One strength of this approach is its consistent applicability throughout the evolution of RTI from linear to nonlinear regimes for all range of Atwood number, $0 < A \leq 1$. In this section, diagnostic parameters of the bubbles at the tip are derived from both in linear and nonlinear regimes. Also, the effect of the finite-size domain kZ on the two diagnostic parameters are examined.

3.1. *Early-time linear dynamics*

The early-time dynamic describes the linear regime where $(t - t_0) \ll \tau$ with $t \gg \tau$ for $t \gg t_0$. In the linear regime, the initial conditions for the curvature $\zeta_1(t_0)$ and the velocity $v_0(t_0)$ are assumed to be small, leading to $0 < |\zeta_1(t_0)k| \ll 1$ and $0 < |v(t_0)(k/g)^{1/2}| \ll 1$. Also, the moments in Eq. (2.10) are approximated to the first order as $M_n = k^n\Phi_1 \sinh(kZ)$, $N_n = k^n\Phi_1 \cosh(kZ)$ and $\widetilde{M}_n = k^n\widetilde{\Phi}_1 \sinh(kZ)$, $\widetilde{N}_n = k^n\widetilde{\Phi}_1 \cosh(kZ)$.

Application of the aforementioned assumptions to the dynamical system in Eq. (2.13) leads to the simplification of the dynamical system as

$$M_0 + \widetilde{M}_0 = 0, \quad \dot{\zeta} - k^2\tfrac{M_0}{2} = 0, \quad \dot{\zeta} + k^2\tfrac{\widetilde{M}_0}{2} = 0,$$
$$(1+A)\left(k\tfrac{\dot{M}_0}{2\tanh(kZ)} - g(t)\zeta\right) = (1-A)\left(k\tfrac{\dot{\widetilde{M}}_0}{2\tanh(kZ)} - g(t)\zeta\right). \tag{3.1}$$

Then, the solution to the dynamical system in the linear regime in Eq. (3.1) is sought as

$$\xi = C_1\sqrt{\frac{t}{\tau}}I_{\frac{1}{2s}}\left(\sqrt{A\tanh(kZ)}\frac{(t/\tau)^s}{s}\right) + C_2\sqrt{\frac{t}{\tau}}I_{-\frac{1}{2s}}\left(\sqrt{A\tanh(kZ)}\frac{(t/\tau)^s}{s}\right) \tag{3.2}$$

$$v = \frac{2}{k}\frac{\mathrm{d}\xi}{\mathrm{d}t}, \tag{3.3}$$

where $s = (a+2)/2$ and I_p is the modified Bessel function of the pth order. Also, ξ is dimensionless curvature defined as $\xi = \zeta/k$. The curvature ζ has a negative value for bubbles as it is concave down $\zeta < 0$ in the considered configuration. We note that bubbles move upward $v > 0$.

The curvature and the velocity for bubbles in the linear regime with the Atwood number $A = 0.7$ are shown in Figure 1. As the acceleration exponent increases from $a = -1$ to $a = 1$, bubbles and spikes are more curved and faster. The effect of the finite-size domain kZ on the velocity v and the curvature ζ_1 are illustrated by comparing the black lines $kZ = 5$ and gray lines $kZ = 0.5$. For the small finite-size domain kZ, v and ζ_1 increase at a slower rate than larger kZ.

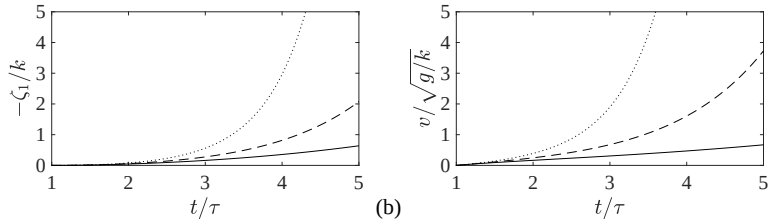

FIGURE 1. Linear regime (a) curvature and (b) velocity for bubbles for pm11. The curvature ζ_1 and the velocity v are shown for the Atwood number $A = 0.7$ with two different finite-size domains, $kZ = 5$ (black lines) and $kZ = 0.5$ (gray lines). The acceleration exponents are $a = -1$ (solid lines), $a = 0$ (dashed line) and $a = 1$ (dotted line).

3.2. *Late-time nonlinear dynamics*

In the linear regime, a unique time-dependent analytic solution for the curvature and velocity was derived. Assuming that the initial velocity and amplitude are small, the moments are retained to the first order. On the other hand, the late-time dynamic under time-varying acceleration in the form of the power-law in Eq. (2.7) shows complicated features compared to the linear regime. For the late-time dynamics, we seek a one-parameter family of asymptotic solutions in the form of the power-law function hinted by the same form of acceleration in Eq. (2.7). In order to derive the asymptoic solution, the following scalings for the terms in Eq. (2.13) are assumed,

$$\zeta_1 \sim k\left(\frac{t}{\tau}\right)^{\beta},\ \Phi_m, \widetilde{\Phi}_m \sim \frac{1}{k\tau}\left(\frac{t}{\tau}\right)^{\alpha},\ \{M, N\} \sim \frac{k^n}{k\tau}\left(\frac{t}{\tau}\right)^{\alpha},\ v \sim \frac{1}{k\tau}\left(\frac{t}{\tau}\right)^{\alpha}, \quad (3.4)$$

where α and β are determined by balancing the conditions of the terms in Eq. (2.13). Substituting Eq. (3.4) for Eq. (2.13) and balancing the exponents of the term lead to two possible pairs of exponents (α, β) depending on the acceleration exponent a.

The power-law exponents of the first pair for RT-type instability ($a > -2$) is $\alpha = \frac{a}{2}$, $\beta = 0$. The power-law exponents of the second pair for RM-type instability ($a < -2$) is $\alpha = -1, \beta = 0$. We note that for the acceleration exponent $a = -2$ the transition from the first case to the second case occurs.

As stated earlier, the present study considers RT-type instability and the acceleration exponents satisfies $a > -2$. Thus, substituting Eq. (3.4) and $\alpha = \frac{a}{2}$, $\beta = 0$ for Eq. (2.13) and retaining only the dominant terms lead to a dynamical system in the nonlinear regime,

$$M_0 + \widetilde{M}_0 = 0, \quad -3N_1\zeta_1 - \tfrac{M_2}{2} = 0, \quad -3\widetilde{N}_1\zeta_1 + \tfrac{\widetilde{M}_2}{2} = 0$$
$$(1+A)\left(\tfrac{N_1^2}{2} - g(t)\zeta_1\right) = (1-A)\left(-\tfrac{\widetilde{N}_1^2}{2} - g(t)\zeta_1\right). \quad (3.5)$$

Note that the acceleration $g(t)$ follows $g(t) = \frac{1}{k\tau^2}\left(\frac{t}{\tau}\right)^a$.

In order to solve the dynamical system in the nonlinear regime in Eq. (3.5), the moments in Eq. (2.10) are truncated to the second order such that $\Phi_m, \widetilde{\Phi}_m = 0$ for $m > 2$ and are substituted for Eq. (3.5). It is worth emphasizing that there are four equations in Eq. (3.5) but there are five unkown variables, $\Phi_1, \Phi_2, \widetilde{\Phi}_1, \widetilde{\Phi}_2$ and ζ_1. Therefore, the solutions for Eq. (3.5) lead to parameterized family solutions, for instance, by the cur-

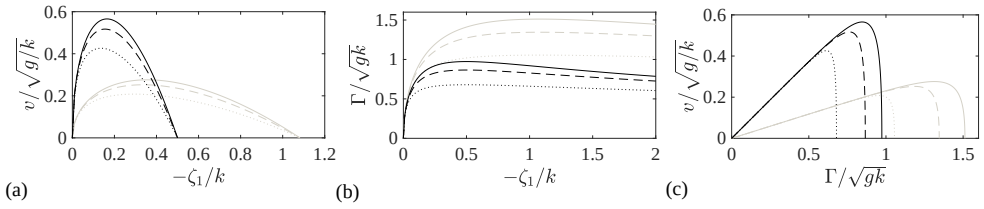

FIGURE 2. The nonlinear regime family of asymptotic solutions for bubbles (a,b,c) for pm11. The velocity $v/\sqrt{g/k}$, the shear $\Gamma/\sqrt{gk}$ and the curvature $\xi = -\zeta_1/k$ are shown with two different finite-domains, $kZ = 5$ (black lines) and $kZ = 0.5$ (gray lines). The Atwood numbers are $A = 0.9$ (solid lines), $A = 0.6$ (dashed lines) and $A = 0.3$ (dotted lines).

vature ζ_1. As solutions to Eq. (3.5), the velocity v and the shear Γ parameterized by ζ_1 are found to be

$$v = \mu \frac{3/\sqrt{2}}{k\tau} \left(\frac{t}{\tau}\right)^{\frac{a}{2}} (A\xi)^{\frac{1}{2}} \frac{\{T_1T_2 + 2(2T_1 - T_2)\xi\}\{T_1T_2 - 2(2T_1 - T_2)\xi)\}}{[(T_1 - 2T_2)^2\{4T_1T_2(2T_1 - T_2)\xi - A(T_1^2T_2^2 + 4(2T_1 - T_2)^2\xi^2\}]^{\frac{1}{2}}}, \tag{3.6}$$

$$\Gamma = \mu \frac{2\sqrt{2}}{\tau} \left(\frac{t}{\tau}\right)^{\frac{a}{2}} (A\xi)^{\frac{1}{2}} \frac{T_1T_2}{[4T_1T_2(2T_1 - T_2)\xi - A\{T_1^2T_2^2 + 4(2T_1 - T_2)^2\xi^2\}]^{\frac{1}{2}}}. \tag{3.7}$$

Here, T_1 and T_2 denote hyperbolic functions, $T_1 = \tanh(kZ)$ and $T_2 = \tanh(2kZ)$. These terms originate from the finite-size domain. Similar to the linear regime solutions in Eq. (3.2) and Eq. (3.3), the dimensionless curvature ξ always remains positive since the curvature ζ_1 is concave down $\zeta_1 < 0$ for bubbles. Moreover, μ determines the sign of the velocity and shear as $\mu > 0$ for bubbles, thus leading to upward propagating bubbles $v > 0$ in the present setup. The solutions are called the one parameter family of asymptotic solution because the velocity v in Eq. (3.6) and the shear Γ in Eq. (3.7) describe all possible velocity and shear solutions parameterized by the curvature, respectively. As can be seen in the form of Eq. (3.6)-(3.7), we note that the solution of bubbles is regular and stable.

Nondimensionalized velocity $v/\sqrt{g(t)/k}$, shear $\Gamma/\sqrt{kg(t)}$ and curvature $\xi = -\zeta_1/k$ for bubbles and spikes are illustrated in Figure 2. The interrelation of three parameters provides many insights into bubble dynamics. RT bubbles span a finite range for the curvature, velocity and shear. In Figure 2(a), bubbles are at the maximum velocity at a certain curvature. Also, static bubble is formed for the maximum possible curvature. Solutions such as Atwood bubbles and flat bubbles can be identified among the family of solutions. As the curvature increases, the velocity drops rapidly at the vicinity of the maximum shear in Figure 2(c).

The effect of the finite-size domain kZ and the Atwood number A is explicitly addressed in Figure 3. Bubbles in the relatively larger domain $kZ = 5$ (black lines) have larger velocity, smaller shear and a small range of permissible curvature bubbles in the relatively smaller domain $kZ = 0.5$ (gray lines). As the Atwood number varies, fluids with a higher contrasting density ($A = 0.9$, solid line) show faster velocity and larger shear than fluids with similar density ($A = 0.3$, dotted line).

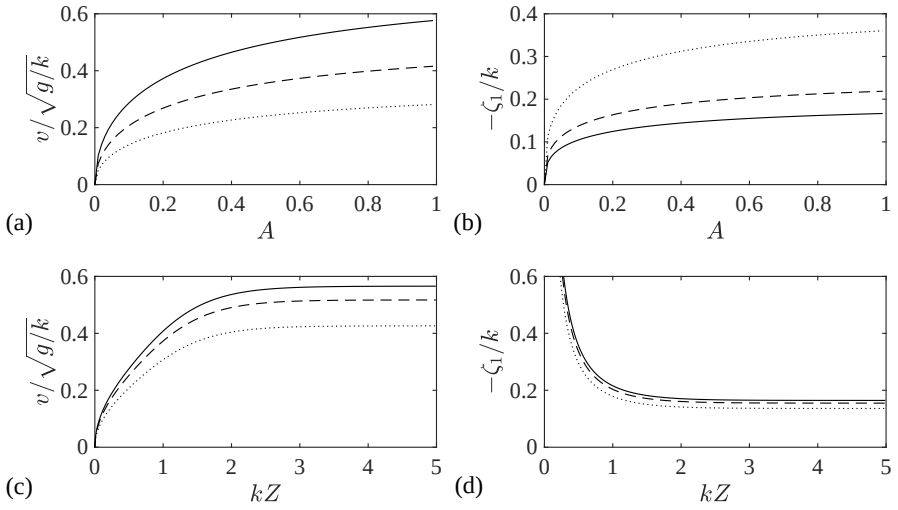

FIGURE 3. The effect of Atwood number A (a,b) and finite-size domain kZ (c,d) on the Atwood bubble curvature ζ_A and the Atwood bubble velocity $v_a/\sqrt{g/k}$ for pm11. Atwood bubble solutions are shown as a function of Atwood number A with three different finite domains, $kZ = 5$ (solid line), $kZ = 1$ (dashed line) and $kZ = 0.5$ (dotted line). The Atwood numbers are $A = 0.9$ (solid line), $A = 0.6$ (dashed line) and $A = 0.3$ (dotted line).

3.3. *Universal scaling*

The effect of the finite-size domain kZ appears in the solutions throughout the linear regime, Eq. (3.3)-(3.2), and the nonlinear regime, Eq. (3.6)-(3.7) as a form of hyperbolic function, such as $\tanh(kZ)$ and $\tanh(2kZ)$. The size of the finite domain kZ is determined as a constant as RTI evolves.

This domain size kZ can be related to the original length scale of RTI, which is the horizontal length scale k. In the linear regime, there exists a scale separation between the height of the large coherent structure h and the finite domain kZ since the initial velocity and amplitude are assumed to be small, and thus, they are independent of each other. On the other hand, in the nonlinear regime, the vertical length scale, h, of bubbles increases to the comparable horizontal length scale of the system, $h \sim O(1/k)$. This similar order of magnitude in length scale implies the possibility of dependence between the characteristic scales, such as k and $g(t)$, and the size of the finite domain kZ.

Following this analogy, the universal scaling bridging the solution in the finite domain to the infinite domain is established for each characteristic scale in the RTI system. In order to demonstrate this universal scaling, we start from the definition of the Atwood bubble. Since the Atwood bubble is the fastest solution, it satisfies

$$\left.\frac{\partial v}{\partial \zeta_1}\right|_{\zeta_1=\zeta_A} = 0, \qquad \left.\frac{\partial^2 v}{\partial \zeta_1^2}\right|_{\zeta_1=\zeta_A} < 0, \tag{3.8}$$

where ζ_A is the curvature ζ_1 for the Atwood bubble and $\zeta_A \in [0, \zeta_{max}]$, where ζ_{max} is the maximum possible curvature for the nonlinear bubble.

In order to compute ζ_A, differentiation of Eq. (3.6) with the curvature ζ_1 leads to the

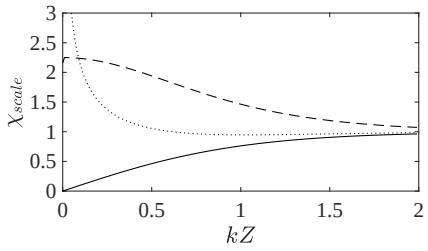

FIGURE 4. Universal scalings as a function of the finite-size domain kZ. Lines are the scaling factors of the length scale $\mathcal{S}_k$ (solid line) and the gravity $\mathcal{S}_g$ (dashed line).

following characteristic equation,

$$48A\left(\frac{2T_1-T_2}{T_1T_2}\xi_A\right)^4+64\left(\frac{2T_1-T_2}{T_1T_2}\xi_A\right)^3+24A\left(\frac{2T_1-T_2}{T_1T_2}\xi_A\right)^2-A=0, \quad (3.9)$$

where $\xi_A=-\zeta_A/k$. Eq. (3.9) implies the form of transformation for length scale, k, as

$$k=\mathcal{S}_k k_\infty, \qquad \mathcal{S}_k=\frac{T_1T_2}{2T_1-T_2}. \quad (3.10)$$

Hereafter, any variables with the subscript ∞ represent a quantity evaluated in the infinite-size domain. Also, $\mathcal{S}_\chi$ denotes the scaling factor linking χ and χ_∞.

In addition, we define the following fundamental scales

$$\mathcal{S}_v=\sqrt{\frac{\mathcal{S}_g}{\mathcal{S}_k}}, \quad \mathcal{S}_\tau=\frac{1}{\sqrt{\mathcal{S}_k\mathcal{S}_g}}, \quad \mathcal{S}_\omega=\frac{1}{\mathcal{S}_\tau}, \quad \mathcal{S}_\lambda=\frac{2\pi}{\mathcal{S}_k}. \quad (3.11)$$

Then, $\mathcal{S}_g$ is derived by substituting Eq. (3.10) for Eq. (3.6) and employing Eq. (3.11) as

$$\mathcal{S}_g=\frac{(T_1T_2)^4}{(T_1-2T_2)^2(2T_1-T_2)^2}, \quad (3.12)$$

and thus, Eq. (3.12) together with Eq. (3.10)-(3.11) define a complete set of fundamental scales in the RTI system.

Especially noteworthy is that the universal scales provide a significant efficiency when describing solutions in the finite domain in terms of simplicity and brevity. For example, the velocity v in Eq. (3.6) and the shear Γ in Eq. (3.7) are rewritten as

$$v_\infty=\mu\frac{3}{\sqrt{2}}\frac{1}{k\tau}\left(\frac{t}{\tau}\right)^{\frac{a}{2}}(A\xi)^{\frac{1}{2}}(1+2\xi)(1-2\xi)\mathcal{D}, \quad \Gamma_\infty=\mu\frac{2\sqrt{2}}{\tau}\left(\frac{t}{\tau}\right)^{\frac{a}{2}}(A\xi)^{\frac{1}{2}}\mathcal{D}, \quad (3.13)$$

where $\mathcal{D}$ is defined as $\mathcal{D}=\left\{4\xi-A(1+4\xi^2)\right\}^{-1/2}$.

Universal scales for the wavelength $\mathcal{S}_k$ and the gravity $\mathcal{S}_g$ are illustrated as a function of the domain size kZ in Figure 4. The finite domain wavelength k increases as the domain size increases, whereas the finite acceleration decreases for a larger domain size.

4. Conclusions

RT dynamics with time-varying acceleration in a finite-size domain for 2D periodic flows is investigated using the group theory. The integrated effects of time-varying acceleration and the finite-size domain are considered for the first time. The acceleration is

assumed to follow the power-law in time. On the basis of the group theory, the stability, the flow structure and isotropy permit only the subspace group pm11. The fluid potentials for heavier and lighter fluids are sought to satisfy the symmetry condition. Then, the dynamical system with moment expressions is obtained. Applying the present approach to solve the dynamical system using group theory allows the solutions to be expanded at the vicinity of the tip of RT bubbles to the desirable accuracy. This approach is consistently used in linear and nonlinear regimes within $0 \leq A \leq 1$. Diagnostic parameters for the large coherent structure of RTI, the velocity and the curvature are demonstrated. Solutions in the linear regime are described as exponential function. Nonlinear regime solutions form a one-parameter family of solutions. The finite size of the domain affects the solution in the nonlinear regime as the structure grows in space. This limitation in space hinders the growth of the structure by an exponent of $\tanh kZ$, where kZ is the nondimensionalized domain size. Moreover, the universal scaling maps the solutions of the infinite-size domain to those of the finite-size domain.

REFERENCES

Abarzhi, S. I. 2008 Review of nonlinear dynamics of the unstable fluid interface: conservation laws and group theory. *Phys. Scr.* **2008**, 014012.

Abarzhi, S. I. 2010 Review of theoretical modeling approaches of Rayleigh-Taylor instabilities and turbulent mixing. *Philos. Trans. R. Soc. A* **368**, 1809-1828.

Abarzhi, S. I., Gauthier, S. & Sreenivasan, K. R. 2013 Turbulent mixing and beyond: non-equilibrium processes from atomistic to astrophysical scales. *Philos. Trans. R. Soc. A* **371**, 20120435

Abarzhia, S. I., Bhowmickb, A. K., Naveha, A., Pandianb, A., Swisherb, N. C., Stellingwerfc, R. F. & Arnettd, W. D. 2018 Supernova, nuclear synthesis, fluid instabilities, and interfacial mixing. *Proc. Camb. Philos. Soc.* **51**, 162–178.

Abarzhi, S. I. 2019 Interfaces and mixing: non-equilibrium transport across the scales. *PNAS* **116**, 18171.

Abarzhi, S. I. & Williams, K. C. 2020 Scale-dependent Rayleigh–Taylor dynamics with variable acceleration by group theory approach. *Phys. Plasmas* **27**, 072107.

Alon, U., Hecht, J., Ofer, D. & Shvarts, D. 1995 Power laws and similarity of Rayleigh-Taylor and Richtmyer-Meshkov mixing fronts at all density ratios. *Phys. Rev. Lett.* **74**, 534.

Anuchina, N. N., Kucherenko, Y. A., Neuvazhaev, V. E., Ogibina, V. N., Shibarshov, L. I. & Yakovlev, V. G. 1978 Turbulent mixing at an accelerating interface between liquids of different densities. *Izv. Akad. Nauk SSSR Mekh. Zhidk. Gaza* **6**, 157-160.

Chandrasekhar, S. 1955 The character of the equilibrium of an incompressible heavy viscous fluid of variable density. *Proc. Camb. Philos. Soc.* **51**, 162–178.

Cook, A. W. & Dimotakis, P. E. 2001 Transition stages of Rayleigh–Taylor instability between miscible fluids. *J. Fluid Mech.* **443**, 69–99.

Dimonte, G. & Schneider, M. 1996 Turbulent Rayleigh-Taylor instability experiments with variable acceleration. *Phys. Rev. E* **54**, 3740.

Goncharov, V. N. 2002 Analytical model of nonlinear, single-mode, classical Rayleigh-Taylor instability at arbitrary Atwood numbers *Phys. Rev. Lett.* **88**, 134502.

Hill, D. L., Bhowmick, A. K., Ilyin, D. V. & Abarzhi, S. I. 2019 Group theory

analysis of early-time dynamics of Rayleigh-Taylor instability with time varying acceleration. *Phys. Rev. Fluids* **4**, 063905.

Jacobs, J. W. & Catton, I. 1988 Three-dimensional Rayleigh-Taylor instability Part 2. Experiment *J. Fluid Mech.* **187**, 353–371.

Landau, L. D. & Lifshitz, E. M. 1987 *Theory Course I-X*. Pergamon Press.

Layzer, D. 1955 On the instability of superposed fluids in a gravitational flied. *Astrophys. J.* **122**, 1.

Meshkov, E. E. 2013 Some peculiar features of hydrodynamic instability development. *Philos. Trans. R. Soc. A* **371**, 20120288.

Mikaelian, K. O. 2008 Limitations and failures of the Layzer model for hydrodynamic instabilities. *Phys. Rev. E* **78**, 015303.

Naveh, A., Hill, D. L. & Abarzhi, S. I. 2020 Early- and late-time evolution of Rayleigh–Taylor instability in a finite-size domain by means of group theory analysis. *Fluid Dyn. Res.* **52**, 025504.

Novak, G. S., Ostriker, J. P. & Ciotti, L. 2011 Feedback from central black holes in elliptical galaxies: two-dimensional models compared to one-dimensional models. *Astrophys. J.* **737**, 26

Olsona, D. H. & Jacobs, J. W. 2009 Experimental study of Rayleigh–Taylor instability with a complex initial perturbation. *Phys. Fluids* **21**, 034103.

Ramaprabhu, P., Dimonte, G., Woodward, P., Fryer, C., Rockefeller, G., Muthuraman, K., Lin, P.-H. & Jayaraj, J. 2012 The late-time dynamics of the single-mode Rayleigh-Taylor instability. *Phys. Fluids* **24**, 074107.

Rayleigh, L. 1883 Investigation of the character of the equilibrium of an incompressible heavy fluid of variable density *Proc. R. Math. Soc.* **14**, 170-177.

Regan, S. P. et al. 2012 *Phys. Plasmas* **19**, 056307

Swisher, N. C., Kuranz, C., Arnettt, W. D., Hurricane, O., Robey, H., Remington, B. A. & Abarzhi, S. I. 2015 Rayleigh-Taylor mixing in supernova experiments. *Phys. Plasmas* **22**, 102707.

Taylor, G. I. 1950 The instability of liquid surfaces when accelerated in a direction perpendicular to their plane. *Proc. R. Soc. Lond. A* **201**, 192-196.

Youngs, D. L. 1984 Numerical simulation of turbulent mixing by Rayleigh–Taylor instability. *Physica D* **12**, 32-44.